JTTEE5 17:144–155
DOI: 10.1007/s11666-007-9142-4
1059-9630/$19.00 © ASM International

Optimization of Atmospheric Plasma Spray Process Parameters using a Design of Experiment for Alloy 625 coatings

F. Azarmi, T.W. Coyle, and J. Mostaghimi

(Submitted March 8, 2007; in revised form September 18, 2007)

Alloy 625 is a Ni-based superalloy which is often a good solution to surface engineering problems involving high temperature corrosion, wear, and thermal degradation. Coatings of alloy 625 can be efficiently deposited by thermal spray methods such as Air Plasma Spraying. As in all thermal spray processes, the final properties of the coatings are determined by the spraying parameters. In the present study, a D-optimal experimental design was used to characterize the effects of the APS process parameters on in-flight particle temperature and velocity, and on the oxide content and porosity in the coatings. These results were used to create an empirical model to predict the optimum deposition conditions. A second set of coatings was then deposited to test the model predictions. The optimum spraying conditions produced a coating with less than 4% oxide and less than 2.5% porosity. The process parameters which exhibited the most important effects directly on the oxide content in the coating were particle size, spray distance, and Ar flow rate. The parameters with the largest effects directly on porosity were spray distance, particle size, and current. The particle size, current, and Ar flow rate have an influence on particle velocity and temperature but spray distance did not have a significant effect on either of those characteristics. Thus, knowledge of the in-flight particle characteristics alone was not sufficient to control the final microstructure. The *oxidation index* and the *melting index* incorporate all the parameters that were found to be significant in the statistical analyses and correlate well with the measured oxide content and porosity in the coatings.

Keywords coating optimization using DOE, influence of spray parameters, porosity of coatings, APS coatings, oxidation in APS coatings

1. Introduction

Alloy 625 has been extensively used in the aerospace, aeronautic, nuclear, marine, petrochemical, and repair industries due to the good mechanical properties and corrosion resistance at an elevated temperature. Air plasma spraying is one of the most versatile and rapid techniques to deposit protective overlay coatings onto the surface of components to increase their in-service properties especially under severe conditions. A conventional plasma spraying system involves three different steps; formation of plasma flame, powder injection, and splat formation. The fundamental of the process is ''heating up'' the powders above their melting point in a plasma stream and accelerate them toward a substrate. The coating will be formed by the ''build-up'' of ''splats'' resulting from the impact, flattening, and solidification of melted powder particles on the substrate (Ref 1-3).

F. Azarmi, T.W. Coyle, and **J. Mostaghimi**, Mechanical Engineering, University of Toronto, Center for Advanced Coating Technologies, 5 King's College Road, Toronto, Canada M5S 3G8. Contact e-mail: fazarmi@mie.utoronto.ca.

The microstructure of plasma sprayed coatings is a lamellae type structure exhibiting anisotropic behavior. Microstructural features are also affected by defects such as pores and microcracks. A number of studies have related the plasma spray process parameters to the final microstructural properties (Ref 4-6). Due to the high velocity and temperature gradients in the plasma plume, any changes in the process parameters can result in significant changes in the particle properties and consequently in the microstructure of the coating. It has been confirmed that the mechanical properties of coatings are dependent not only on the deposition method but also on the choice of process operational parameters for a given coating method.

As a basic requirement for increasing coating quality, operational process variables must be optimized. The optimization can be a very complex and time-consuming process. Therefore, a Design of Experiments (DOE) approach for the optimization of processing parameters for coating structures is commonly employed (Ref 7, 8). The statistically designed experiments and multiple regression analysis are used to determine the effects of processing parameters on mechanical and microstructural properties of coatings. The effect of changing the processing parameters on properties such as hardness, density, thickness, and the amount of porosity in the coatings has been investigated in these reports.

Information about the in-flight particle characteristics such as velocity (V_p) and temperature (T_p) contributes to a better understanding of the process of deposit build-up. Previous investigations have described how the in-flight

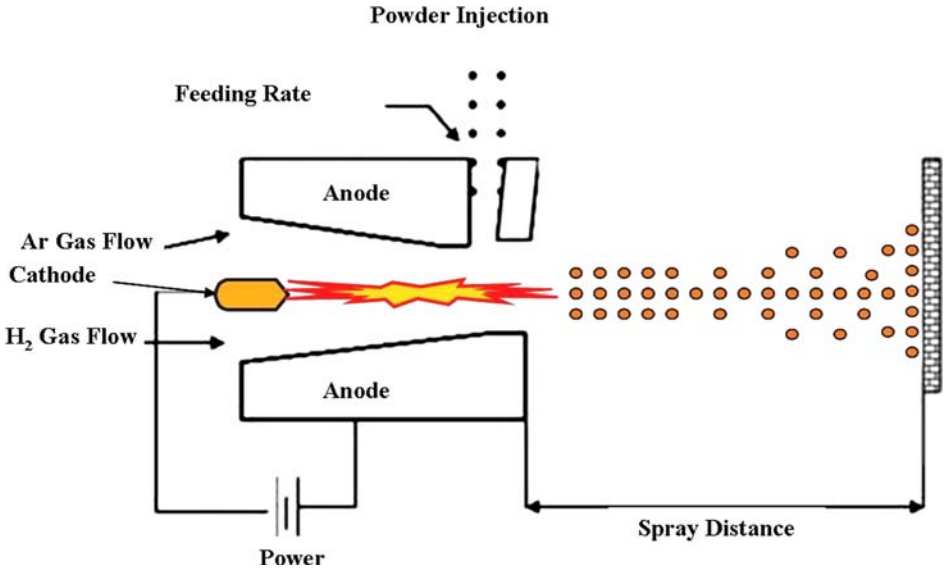

Fig. 1 Schematic of APS system with illustration of parameters varied in designed experiments

temperature and velocity of the powder particles influence splat morphology by affecting the flattening, oxidation, and solidification processes (Ref 9). These, in turn, ultimately affect the final microstructure and properties of the coating itself. Friis et al., suggested that the microstructural variations in the final coating could be better correlated with the in-flight particle properties than with the spraying process parameters (Ref 10). Recently developed online particle monitoring systems have made it possible to measure in-flight particle properties at any distance from the gun to the substrate. The distribution in the velocity, temperature, and size of individual particles can be measured as a function of position within the plasma plume during the deposition process.

The objective of this work was to produce dense, single-phase coatings. Two sets of experiments were conducted. A custom experimental design approach with variables at two levels was used for the first set of experiments. The impact of powder size and five other important plasma-spraying variables: current, primary plasma gas (Ar) flow, hydrogen gas flow, spraying distance, and powder feed rate was studied. A second set of coatings were deposited employing the optimal spraying parameters predicted from the results of the first set of experiments to confirm the validity of the statistically based model. Figure 1 shows a schematic of the APS system and the process parameter variables used in the experimental design.

2. Experimental Procedure

2.1 Materials

Two different commercially available spheroidal, gas atomized powders of composition similar to Inconel 625, Metco AMDRY 625 and Metco Diamalloy 1005, were used for these experiments. The nominal composition for both powders was 21.5 wt.% Cr, 8.5 wt.% Mo, 3 wt% Nb, 3 wt.% Fe, 0.5 wt.% Co, and remainder Ni. The nominal particle size is in the range of (−90 to +45 μm) for AMDRY 625 and (−45 to +11 μm) for Diamalloy 1005. SEM images of both types of powders used in this investigation are shown in Fig. 2(a) and (b). Figure 2(c) compares the size distribution of the AMDRY 625 and DIAMALLOY 1005. The average particle sizes for these powders were 78 μm and 25 μm, respectively, measured by particle size analysis, Mastersizer S from Malvern Instruments Ltd., UK.

2.2 Air Plasma Spraying Process

An SG-100 plasma spray gun (Miller Thermal Inc., WI, USA) mounted on a computer-controlled robotic arm was used to deposit the alloy 625 coatings at atmospheric pressure. Coatings 200-300 μm thick were deposited on grit blasted, rectangular shaped mild steel substrates, 22 mm L × 8 mm W × 2.5 mm T. The substrates were cooled by air jets during the spraying process. The substrate temperature was not normally measured during deposition in this study.[1] Ar was used as the powder carrier gas at a flow rate of approximately 9 sl/min. During some spraying runs the velocity and temperature of in-flight particles were measured using a DPV 2000 (Tecnar Automation Ltée, QC, Canada). The DPV 2000 workstation consists of a sensing head and optical cable attached to a detection module linked to a computerized control system. The optical sensing head device contains a two-slit photo mask. Particle velocity is determined by time of flight between the two slits. The particle temperature measurement is based on two-color pyrometry theory. Prior to the measurement, the sensing head must be

[1]The substrate temperature was measured using a thermocouple attached to the back of the substrate during deposition under the conditions selected as optimal at the conclusion of the study (run Z in Table 7) and found to plateau at approximately 610 K.

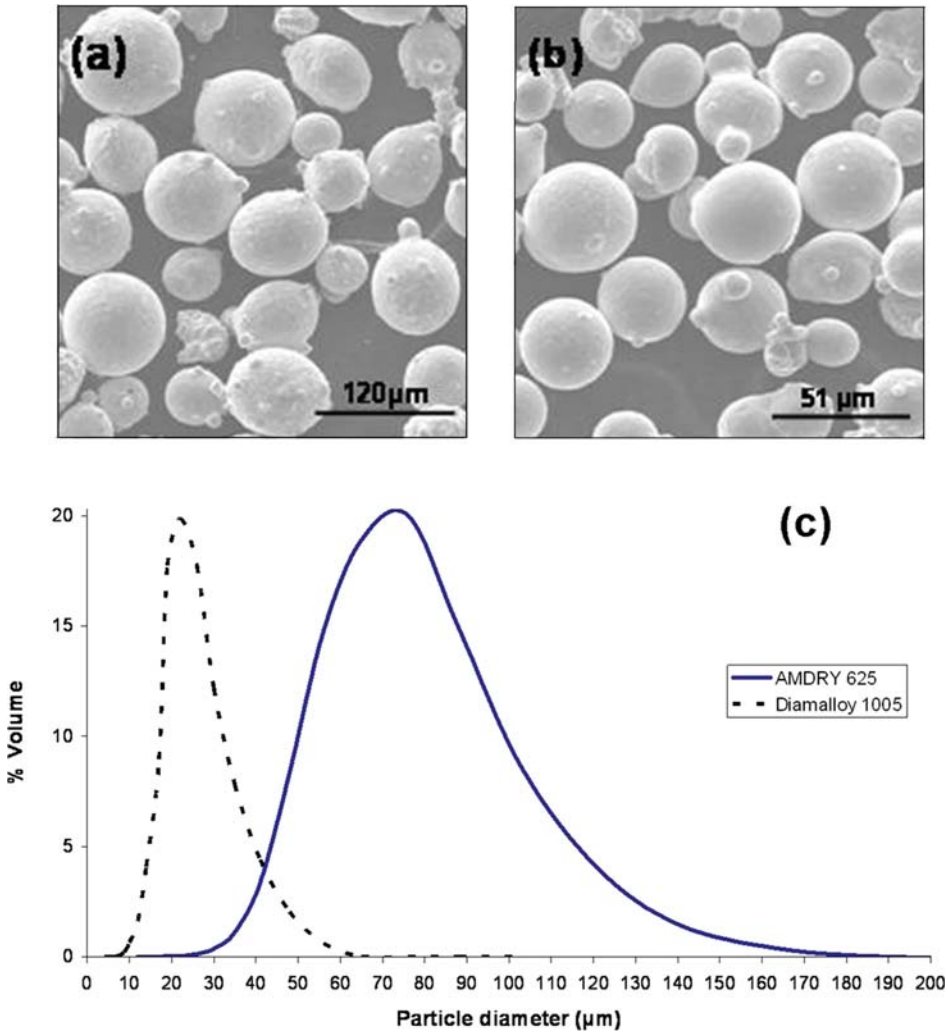

Fig. 2 Alloy 625 powders used for APS spraying. (a) Metco-AMDRY 625-78 µm, (b) Metco-DIAMALLOY 1005-25 µm, and (c) Powder size distribution

aligned with respect to the torch axis in both the horizontal and vertical directions at the specific spray distance in the absence of the substrate. Alignment was performed using the auto-centering function of the DPV 2000, which aligns the sensing head with the point of highest particle density in the plume at the specified spray distance. As powder injection needs a certain amount of time to reach dynamic equilibrium, measurements began only after a stable plume is achieved. Figure 3 shows a schematic of the DPV 2000 operational set-up.

2.3 Initial Set of Experiments

Some experimental studies have suggested applicable ranges of operational spraying parameters for Ni-based superalloy materials (Ref 11-13). Commercially available data analysis software JMP from SAS Institute Inc., USA, was used to construct a D-optimal design for the first set of experiments to determine optimum operating conditions with a minimum number of runs. This type of computer-aided design is particularly useful when classical designs do not apply. One of the advantages of this design is the capability to create models which target specific interaction terms. The optimality criterion results in minimizing the generalized variance of the parameter estimates for a pre-specified model. Unlike standard classical designs such as fractional factorials, D-optimal design matrices are usually not orthogonal and effect estimates are correlated (Ref 14). A total of eight experimental runs were required to provide enough information to develop a model to predict the porosity and oxide content taking into account all first order single factor effects. Table 1 presents the eight experimental runs generated.

2.4 Coating Characterization

The coating samples were cross-sectioned using a diamond-coated blade prior to the microscopic observations and hardness tests. Cut samples were mounted using cold epoxy under low pressure to minimize pull out of particles during preparation. Then, the samples were ground using 320-800 grit SiC papers followed by 9, 3, and 1 µm

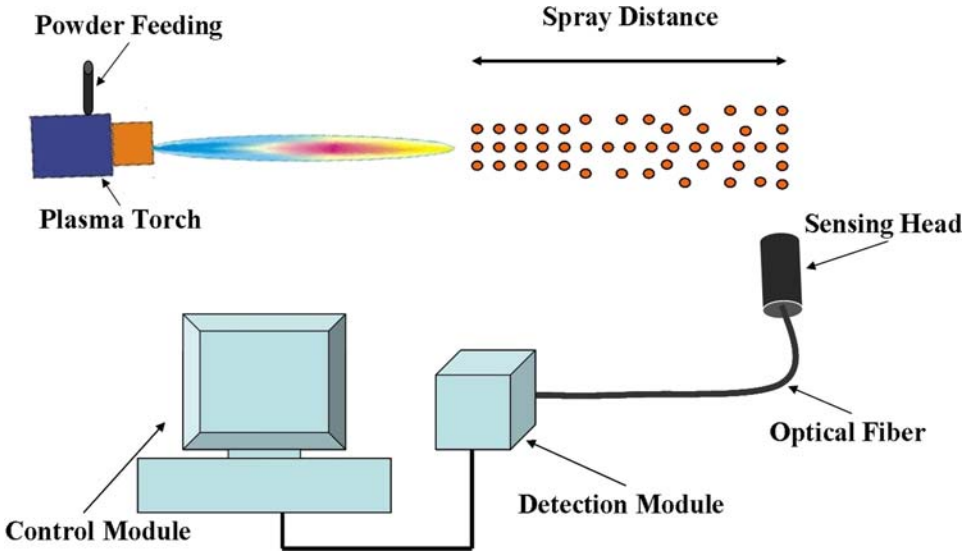

Fig. 3 Schematic of the DPV 2000 operational set-up

Table 1 Plasma spraying process parameters for the first set of experiments

Run	Powder size, μm	Spray distance, mm	Feed rate, g/min	Current, A	Voltage, V	Power, KW	Ar, sl/min	H_2, sl/min
A	25	50	48	750	45	33.75	55	2
B	78	50	48	550	34	22.1	65	0
C	78	75	48	550	41	26.65	55	2
D	25	75	48	750	39	29.25	65	0
E	25	50	28	550	33	21.45	55	0
F	25	75	28	550	47	30.55	65	2
G	78	50	28	750	45	33.75	65	2
H	78	75	28	750	35	26.25	55	0

diamond suspensions and finished with an 0.05 μm alumina suspension as polishing agents. The microstructure characterizations have been performed using an S-570, Hitachi, Tokyo, Japan scanning electron microscope to obtain photomicrographs of coatings. Elemental analysis for elements of atomic number 11 and above was carried out on a Link Analytical LZ-5. Electron probe microanalysis (EPMA) was performed using a CMECA electron probe microanalyzer equipped with an SX-50 X-ray detector to detect the presence of oxygen. Image analysis software, from Clemex Technologies Inc., Canada was used to determine the amount of porosity and oxide phases in the coatings from the 20 SEM images with a magnification of 700× taken at distinct locations on each coating sample.

The Knoop hardness of each sample was measured using a Zwick microhardness machine under an applied load of 9.8 N for 25 s. Ten indentation tests were performed on each coating cross section, with the long axis of the indent oriented perpendicular to the deposition direction.

2.5 Validation Runs

The amount of porosity and oxide phases obtained from the first set of experiments was used to develop empirical models (Eq 1-3) relating the deposition conditions to the coating structure. These models were used to predict the porosity, oxide content, and hardness to be expected as a function of variation of the factors. In the predictions, all factors were defined as continuously variable between the two limits specified in the original experimental design, except the powder particle size and spray distance, which were limited to the two specific values. The process parameter values used in the models are given in Table 2.

Oxide content was predicted from the following expression derived from the results of the first set of experiment:

$$\left[\begin{array}{l}\text{Oxide Content } \% = 12.2 + \text{Match [Powder Size]} \begin{bmatrix} \text{“25 μm”} \Rightarrow 7 \\ \text{“78 μm”} \Rightarrow -7 \\ \text{else} \Rightarrow 0 \end{bmatrix} + \text{Match [Spray Distance]} \begin{bmatrix} \text{“50 mm”} \Rightarrow -2 \\ \text{“75 mm”} \Rightarrow 2 \\ \text{else} \Rightarrow 0 \end{bmatrix} \\ \quad - 0.03 \times \dfrac{[\text{Feed Rate(g/min)} - 38]}{10} + 0.7 \times \dfrac{[\text{Current (A)} - 650]}{50} + 1.8 \times \dfrac{[\text{Ar Gas Flow (sl/min)} - 60]}{5} \\ \quad + 0.5 \times [H_2 \text{ Gas Flow (sl/min)} - 1] \end{array}\right] \quad \text{(Eq 1)}$$

Porosity in the coating was predicted from the following expression:

$$\left[\begin{array}{l}\text{Porosity \%} = 0.8 + \text{Match [Powder Size]}\begin{bmatrix}\text{“25 μm”} \Rightarrow -0.16\\ \text{“78 μm”} \Rightarrow 0.16\\ \text{else} \Rightarrow 0\end{bmatrix} + \text{Match [Spray Distance]}\begin{bmatrix}\text{“50 mm”} \Rightarrow 0.21\\ \text{“75 mm”} \Rightarrow -0.21\\ \text{else} \Rightarrow 0\end{bmatrix}\\ \quad + 0.08 \times \dfrac{[\text{Feed Rate (g/min)} - 38]}{10} + 0.16 \times \dfrac{[\text{Current (A)} - 650]}{50} + -0.04 \times \dfrac{[\text{Ar Gas Flow (sl/min)} - 60]}{5}\\ \quad + 0.08 \times [\text{H}_2\text{ Gas Flow (sl/min)} - 1]\end{array}\right] \quad \text{(Eq 2)}$$

Similarly, hardness was predicted from:

$$\left[\begin{array}{l}\text{Hardness (Knoop)} = 317 + \text{Match [Powder Size]}\begin{bmatrix}\text{“25 μm”} \Rightarrow 50.1\\ \text{“78 μm”} \Rightarrow -50.1\\ \text{else} \Rightarrow 0\end{bmatrix} + \text{Match [Spray Distance]}\begin{bmatrix}\text{“50 mm”} \Rightarrow -2.4\\ \text{“75 mm”} \Rightarrow 2.4\\ \text{else} \Rightarrow 0\end{bmatrix}\\ \quad - 3.8 \times \dfrac{[\text{Feed Rate (g/min)} - 38]}{10} + 13.1 \times \dfrac{[\text{Current (A)} - 650]}{50} + 0.375 \times \dfrac{[\text{Ar Gas Flow (sl/min)} - 60]}{5}\\ \quad + 24.6 \times [\text{H}_2\text{ Gas Flow (sl/min)} - 1]\end{array}\right] \quad \text{(Eq 3)}$$

Table 2 Process parameters for validation run

	Powder size, μm	Spray distance, mm	Feed rate, g/min	Current, A	Ar, sl/min	H_2, sl/min
Process parameters	25, 78	50, 75	28, 33, 38, 43, 48	550, 600, 650, 700, 750	55, 57.5, 60, 62.5, 65	0, 0.5, 1, 1.5, 2

The six combinations of process parameters predicted to yield the lowest apparent porosity were used to deposit a second set of coatings. The measured apparent porosity and fraction of oxide phases and the hardness for this set of spraying runs were compared to the predictions to test the validity of the DOE model.

3. Results and Discussion

3.1 First Set of Experiments

3.1.1 In-flight Particle Characteristics. The influence of the spraying process parameters on the in-flight temperature and velocity of the powder for the first set of runs is shown in Table 3. The Pareto diagram shown in Fig. 4 illustrates the effects of the various parameters on the in-flight particle temperature during spraying. The effect of a parameter is significant at a 95% confidence level if the absolute value of the coefficient for that parameter crosses the dashed line. Powder size is the only spraying parameter which has a significant effect on the in-flight particle temperature according to Fig. 4, with the small particle size powder yielding higher particle temperatures than the large particle size powder. The next most important parameters are the H_2 and Ar gas flow rates, which are significant at approximately the 85% confidence level.

Table 3 In-flight particles temperature and velocity for the first set of experiments

Run	Powder temperature, K	Powder velocity, m/s
A	2673 ± 120	130 ± 30
B	2173 ± 120	90 ± 30
C	2473 ± 160	70 ± 20
D	2573 ± 160	110 ± 20
E	2573 ± 180	130 ± 20
F	2673 ± 100	120 ± 20
G	2373 ± 170	70 ± 20
H	2473 ± 180	100 ± 20

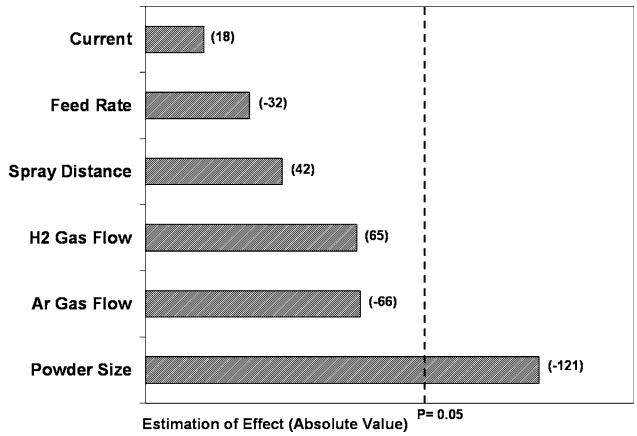

Fig. 4 Pareto diagrams showing the effects of process parameters on the in-flight particle temperature

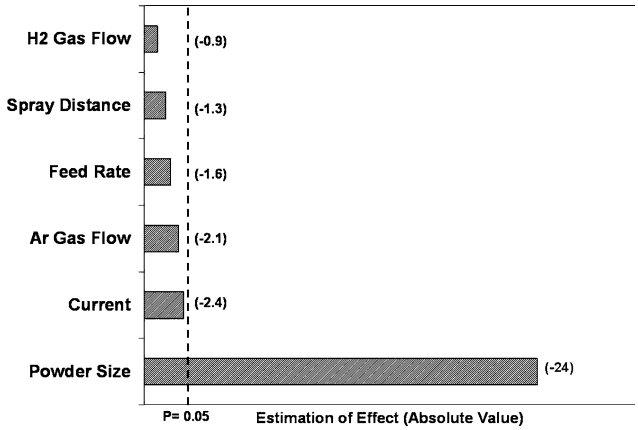

Fig. 5 Pareto diagram showing the effects of process parameters on the in-flight particle velocity

Figure 5 shows a Pareto diagram for the in-flight particle velocities during spraying. Again, only the effect of powder size is significant at the 95% confidence level, with small particles having higher velocities. The current and Ar gas flow rate are also significant at approximately the 90% confidence level.

3.1.2 Coating Characterization. SEM images of polished cross sections of coatings deposited in the experimental runs A-H are shown in Fig. 6. Areas of three discernable levels of contrast were seen. The darkest regions were identified as pores. Additional characterization was conducted to determine the composition of the areas of intermediate contrast. EDS was used to determine composition of each region according to the level of contrast. The average composition of the light contrast region was found to be approximately 66 wt.% Ni, 21 wt.% Cr, 8 wt.% Mo, 2 wt.% Nb, and 1.4 wt.% Fe, which was very close to that of the initial powder. EDS results indicate that the major elements in the intermediate contrast regions are chromium and oxygen. The average composition of the light contrast region was found to be approximately 11 wt.% Ni, 44 wt.% Cr, 12 wt.% Mo, 9 wt.% (Nb + Fe), and about wt.% 23 oxygen. EDS results for regions of light and intermediate contrast regions in the coating deposited in experiment D is shown in Fig. 7.

Table 4 Hardness, secondary oxide phase content, and porosity

Run	% Oxide phase (Intermediate contrast)	% Porosity (Dark area)	Hardness (Knoop)
A	15 ± 1.3	0.6 ± 0.19	408 ± 15
B	2 ± 0.13	1.5 ± 0.2	185 ± 21
C	5 ± 0.74	0.6 ± 0.09	312 ± 24
D	24 ± 1.17	0.2 ± 0.09	379 ± 11
E	14 ± 1.01	0.7 ± 0.1	300 ± 24
F	21 ± 0.9	0.5 ± 0.1	327 ± 15
G	6 ± 0.57	0.6 ± 0.08	267 ± 16
H	4 ± 0.34	0.6 ± 0.11	195 ± 18

It has been previously reported that due to the entrainment of the surrounding air into the plasma jet, the existence of an oxide phase in APS metal coatings is not unexpected (Ref 15). It is generally believed that the reaction between the particle and its surrounding atmosphere is controlled by diffusion. If the Reynolds number of the flow relative to particles is higher than 20 and particles are completely molten, the oxidation process is governed by convective movement of particles and oxygen adsorption at the surface of particles (Ref 2). Table 4 shows the amount of oxide phase, porosity, and hardness for each experiment. The amount of oxide phase in coating increases with the increase in spray distance. It indicates that the main oxidation occurs during the particle flight from the gun toward substrate. Edris and McCartney has also reported existence of such an oxide phase for plasma sprayed alloy 625 (Ref 16).

EPMA results show a very high oxygen concentration in the regions of intermediate contrast compared to the light areas as shown in Fig. 8, indicating the existence of a chromium oxide in those regions. The hardness increases drastically with increase in the amount of intermediate contrast regions in the microstructure, consistent with the presence of a hard oxide phase.

The effects of the operating parameters on the oxide phase content in the coatings are shown in the Pareto chart of Fig. 9. Here, three parameters are significant at the 95% confidence level: powder size, spray distance, and Ar flow rate. The particle size has the largest effect on the amount of oxide phase in the coating. This is consistent with the higher temperature of the small size particles and their larger surface area compared to the coarse powder. The additional statistically significant factors which influence the oxide content in the deposits indicate that knowledge of the particle temperature and velocity at the point of impact is not sufficient to control the oxide content in the deposit.

The effects of the operating parameters on the porosity are shown in the Pareto chart of Fig. 10. The three parameters which are significant at the 95% confidence level are spray distance, powder size, and current. Porosity decreased with increased spray distance, smaller particle

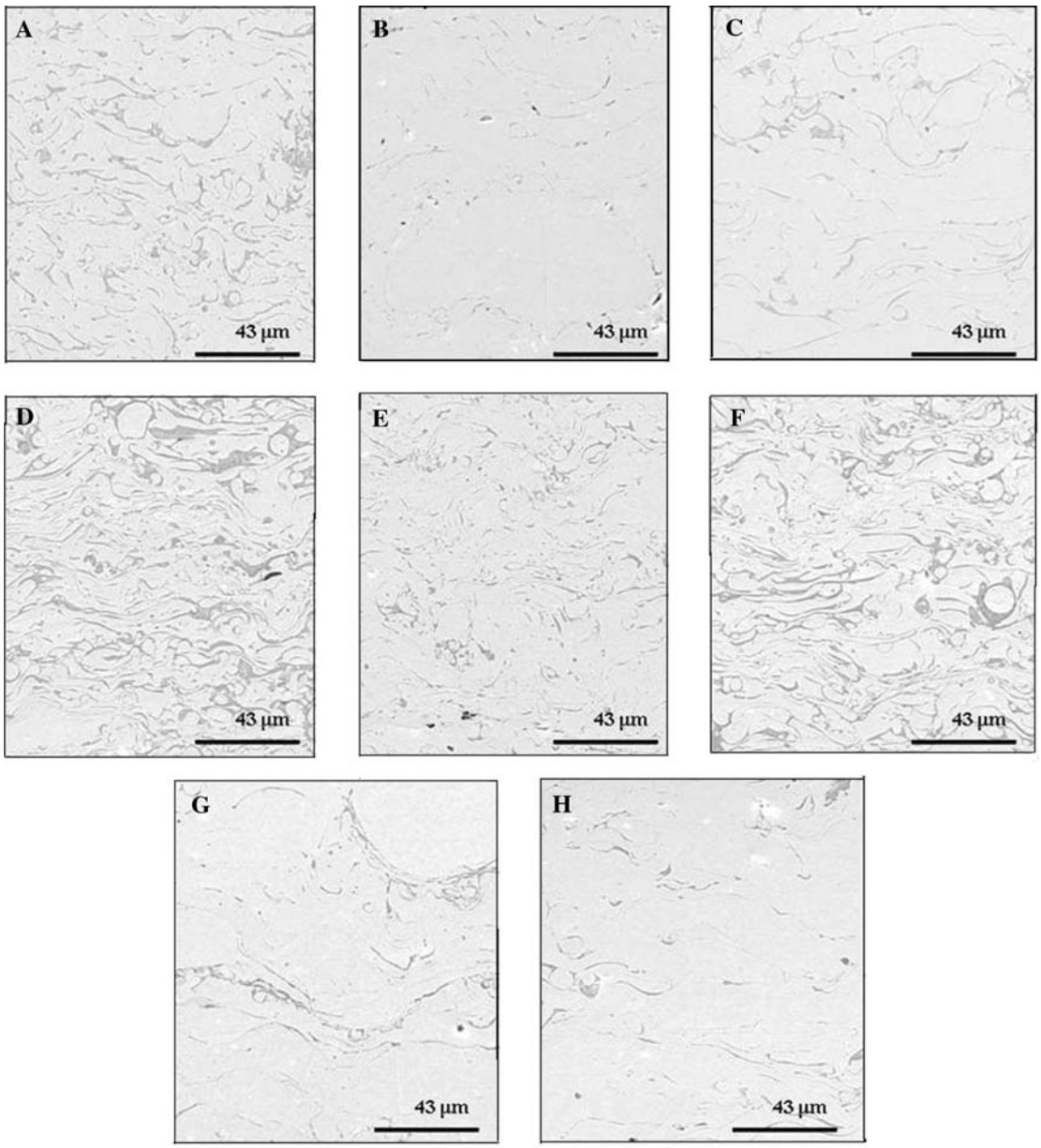

Fig. 6 The microstructure of coatings (A-H) resulting from first set of experiments

size, and lower current. Again, the particle temperature and velocity at the point of impact do not appear to completely explain the porosity variations.

3.2 Model Validation Experiments

3.2.1 Predicted Optimal Process Parameters. The second set of experiments was designed from the empirical model established from the results described above. The porosity, oxide content, and hardness were predicted from the model for over 2000 combinations of deposition parameters as described in Sect. 2.5. The six combinations of process parameters which yielded the lowest predicted oxide contents and porosities, with the emphasis on oxide content, were chosen according to Fig. 11. The values of the parameters for these runs along with the predicted oxide contents and hardness values are shown in Table 5.

3.2.2 In-flight Particle Characteristics. The in-flight characteristics of the particles measured during deposition are shown in Table 6. The process parameters varied in these experiments which were found to have significant effects on the in-flight particle temperature and velocity in the first set of experiments, were hydrogen gas flow and current, respectively. The effect on particle temperature is apparent in the second set of experiments, however the variation in particle velocity is small. The temperatures and velocities of the particles in-flight are in the intermediate range of those given in Table 3.

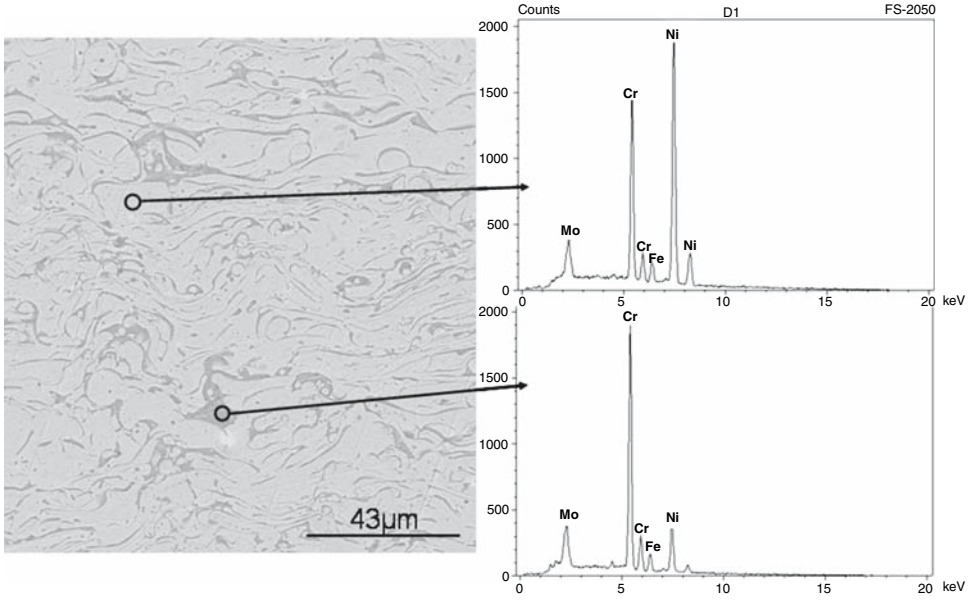

Fig. 7 EDS results for regions of intermediate and light contrast in the coating deposited in experiment D

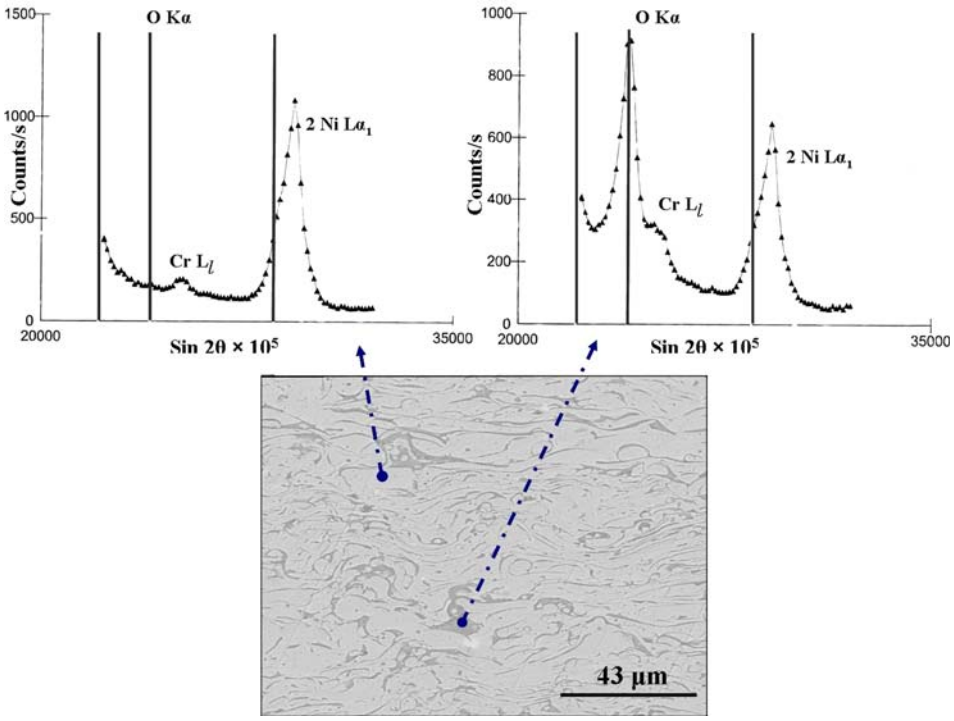

Fig. 8 EPMA results for oxygen in regions of intermediate and light contrast in the coating deposited in experiment D

3.2.3 Coating Characterization. Features resulting from six spraying processes using parameters indicated in Table 5 are shown in the SEM micrographs of Fig. 12. The SEM micrographs are taken from polished and unetched cross section of coatings Z-U. Three levels of contrast can be discerned in the images. The darkest features were identified as pores. The intermediate constant areas were again identified to be a chromium oxide phase using EDS on the SEM. Image analysis indicates that the amount of oxide phase was lower in the coatings produced in the second set of experiments compared to those from the first set of experiments. It also illustrates that the amount of porosity was slightly increased in coatings produced in the second set of experiments, particularly the large equiaxed

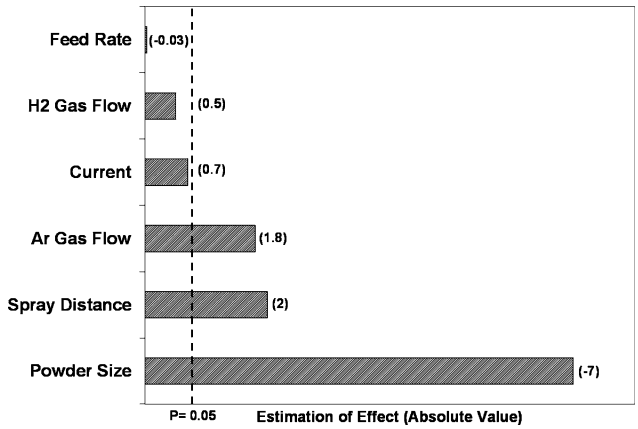

Fig. 9 Pareto diagram showing the effects of process parameters on the oxide phase content

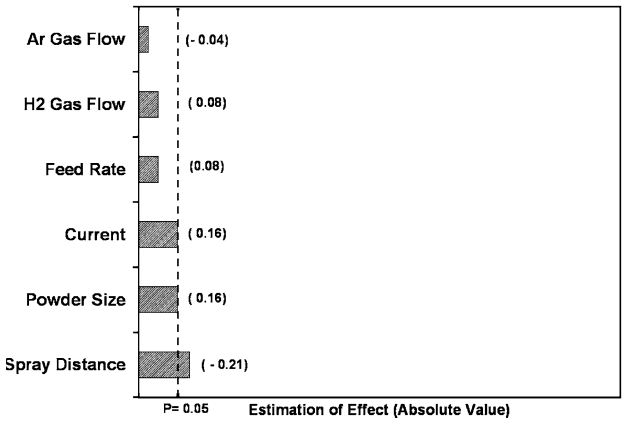

Fig. 10 Pareto diagram showing the effects of process parameters on the porosity

pores, compared to the coatings previously deposited under conditions yielding higher average particle temperatures.

The number of unmelted or partially melted particles within the microstructure of coatings Z-U was also larger than in the coatings previously deposited under conditions yielding higher average particle temperatures. The increase in the number of large pores and unmelted particles is more visible in the coatings produced from experiments V and U. Figure 13(a) illustrates an unmelted particle from inside the cross section of coating V and (b) shows a single unmelted particle from U which is not completely attached to the coating.

A comparison between the predicted and experimental results is shown in Table 7. In most instances, the predicted oxide contents, porosity, and hardness values fall within the range of scatter in the measured values. The coating produced from experiment V yielded the minimum in both predicted and experimental oxide content. However, these conditions also resulted in a large number of unmelted particles within the coating, higher porosity, and low cohesion between lamellae. To fully optimize the deposition conditions, both oxide content and porosity must be minimized simultaneously. Coatings X and Z appear to best satisfy this combined criterion, with slightly higher oxide content than run V but lower porosity. These coatings also exhibited better adhesion and cohesive strength.

3.3 Discussion

It is generally accepted that particle temperature and velocity at the point of impact (for a given substrate or deposit temperature) play a dominant role in determining the shape of individual splats and the structure of a thermal spray coating. In these experiments, the particle size was the dominant parameter affecting the in-flight particle velocity and temperature. The next most important parameters for the particle velocity were current and Ar flow rate, while the Ar and H_2 flow rates were the next most important parameters for the particle temperature.

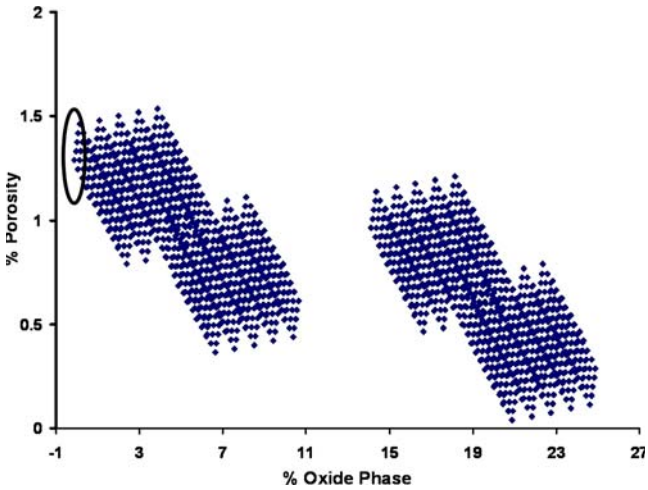

Fig. 11 Prediction resulting model for oxide phase and porosity used for second set of experiment

The deposition parameters which exhibited the most important effects directly on the oxide content in the coating were particle size, spray distance, and Ar flow rate. The effects of particle size and Ar flow rate can be understood in terms of their influence on particle velocity and temperature; however, spray distance did not have a significant effect on either of those in-flight particle characteristics. The parameters with the largest effects directly on porosity were spray distance, particle size, and current. Similarly, the effects of particle size and current can be attributed to their influence on the in-flight particle conditions, but spray distance, which did not significantly affect the in-flight characteristics, had the largest influence on porosity.

Xiong et al. (Ref 17) have derived an *oxidation index* based on a simplified model of the oxidation kinetics of a molten droplet in-flight, assuming convective transport of oxygen from the plasma gas to the surface of the droplet as the rate-limiting step:

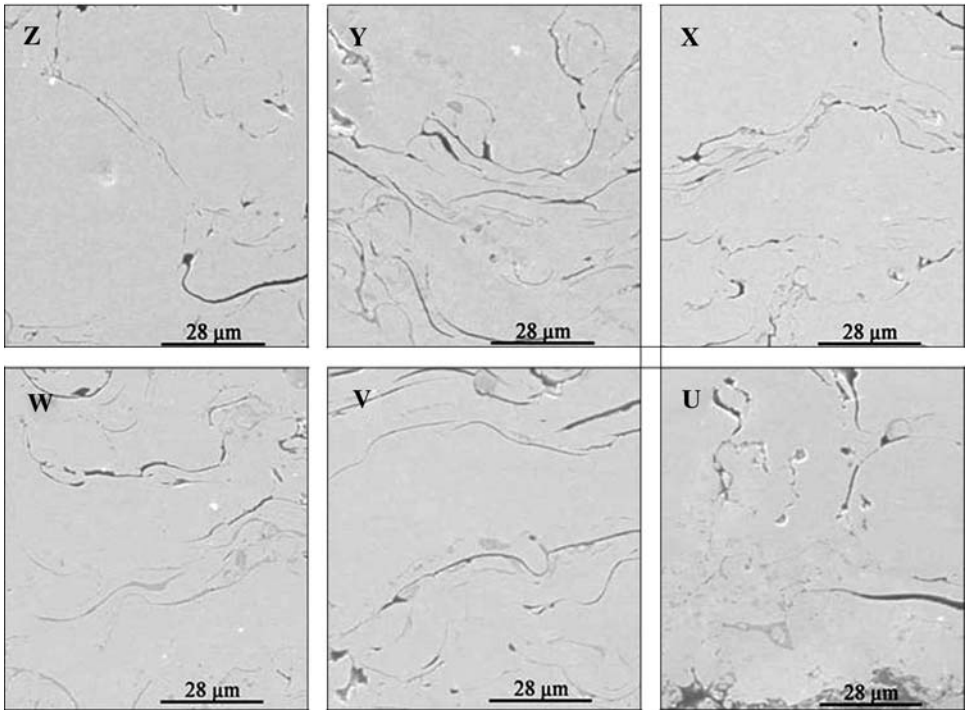

Fig. 12 The microstructure of coatings (Z-V) from the second set of experiments

Table 5 Plasma spraying process parameters selected for the second set of experiments with predicted values for secondary oxide phase and hardness

Run	Powder size, μm	Spray distance, mm	Feed rate, g/min	Current, A	Ar, sl/min	H_2, sl/min	Predicted porosity, %	Predicted oxide phase, %	Predicted hardness (Knoop)
V	78	50	28	550	55	0	1.6	1.6	217
X	78	50	28	600	55	0	1.4	1.7	221
Z	78	50	28	630	55	0	1.3	1.9	230
U	78	50	28	550	55	1	1.5	2.8	228
W	78	50	28	600	55	1	1.3	3.1	242
Y	78	50	28	630	55	1	1.2	3.6	255

Table 6 In-flight particles temperature and velocity for the second set of experiments

Run	Powder temperature, K	Powder velocity, m/s
V	1973 ± 240	90 ± 20
X	2173 ± 210	100 ± 30
Z	2073 ± 240	100 ± 30
U	2273 ± 170	80 ± 20
W	2573 ± 170	110 ± 30
Y	2473 ± 180	90 ± 30

$$\text{oxidation index} \propto \frac{S}{V_p D_p^2} \quad \text{(Eq 4)}$$

where S is the spay distance, V_p is the particle velocity, and D_p is the particle diameter. The *index* includes the three factors which were found to have the most significant effect on oxide content in the present experiments, recognizing that particle velocity is itself largely determined by Ar flow rate and particle size. When the measured oxide content is plotted versus the *oxidation index*, an excellent correlation is obtained for both the first and second sets of experiments and for large and small particle size powders, Fig. 14.

Table 7 Experimental results for hardness, oxide phase, and porosity for coatings produced in the second set of experiments

Run	% Oxide phase predicted	% Oxide phase	% Porosity predicted	% Porosity	Hardness (Knoop) predicted	Hardness (Knoop)
V	1.6	1.9 ± 0.4	1.6	3 ± 1	217	166 ± 16
X	1.7	2.8 ± 0.6	1.4	2 ± 0.7	221	199 ± 20
Z	1.9	2.9 ± 0.6	1.3	1.6 ± 0.9	230	203 ± 18
U	2.8	3.6 ± 0.7	1.5	2.9 ± 0.6	228	212 ± 17
W	3.1	3.4 ± 0.4	1.3	1.9 ± 0.8	242	230 ± 25
Y	3.6	4.9 ± 0.8	1.2	0.9 ± 0.6	255	266 ± 26

Vaidya et al. (Ref 18) have proposed the use of in-flight particle parameters to describe the particle state; known as the *melting index* it is given as follows:

$$\text{Melting index} = T_s \cdot \frac{\Delta t_{fly}}{D_p} \quad \text{(Eq 5)}$$

where T_s is the in-flight particle temperature, Δt_{fly} is the residence time for the particle in-flight, and D_p is the particle diameter. Assuming that the particles undergo constant acceleration from zero to their final velocity, the particle residence time is approximated as $\Delta t_{fly} = 2S/V_p$, where S is the spray distance and V_p is the particle velocity. When the measured porosity content is plotted versus the *melting index*, a good correlation is obtained for both the first and second sets of experiments and for large and small particle size powders, Fig. 15. This graph indicates that with increase in the *melting index*, the porosity decreases. It can also be seen from the graph that when the *melting index* is less than 0.03, the porosity increases rapidly.

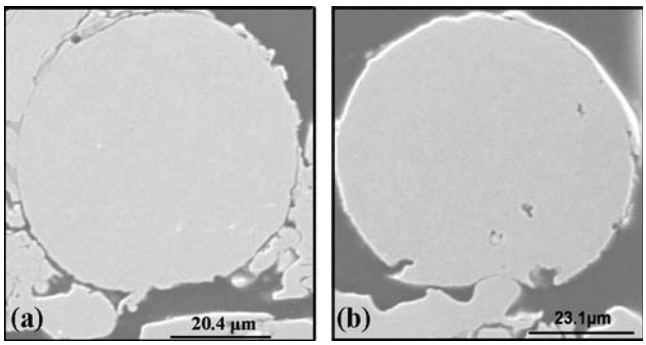

Fig. 13 (a) A trapped unmelted particle within the coating (experiment V), and (b) an unmelted particle separated from coating (experiment U)

4. Summary and Conclusions

The effects of powder size, spray distance, current, carrier gas flow, and H_2 gas flow on the porosity and formation of oxide phase have been investigated for alloy 625 coatings deposited by atmospheric plasma spraying. A D-optimal experimental design was used to characterize the effects of the APS process parameters on in-flight particle temperature and velocity, and on the oxide content and porosity in the coatings. These results were used to create an empirical model to predict the optimum deposition conditions. A second set of coatings was then deposited to test the model predictions.

The powder size has the largest effect on the in-flight particle temperature. Process parameters such as Ar and H_2 gas flow rate can be considered as the next most important parameters influencing the particle temperature. The most important variable affecting the in-flight velocity is powder size, while current and Ar gas flow rate are also significant. However, the experimental results do not provide a systematic map for the effect of the in-flight properties on the final microstructure.

The empirical model successfully predicted deposition parameters which simultaneously minimized the oxide content and porosity in the second set of coatings. The optimum spraying conditions produced a coating with less than 4% oxide and less than 2.5% porosity. The hardness of that coating was approximately 200 HK, within the range commonly found for bulk alloys of this composition (Ref 19).

The process parameters which exhibited the most important effects directly on the oxide content in the coating were particle size, spray distance, and Ar flow rate. The particle size and Ar flow rate have an influence on particle velocity and temperature but spray distance did not have a significant effect on either of those in-flight particle characteristics. The parameters with the largest

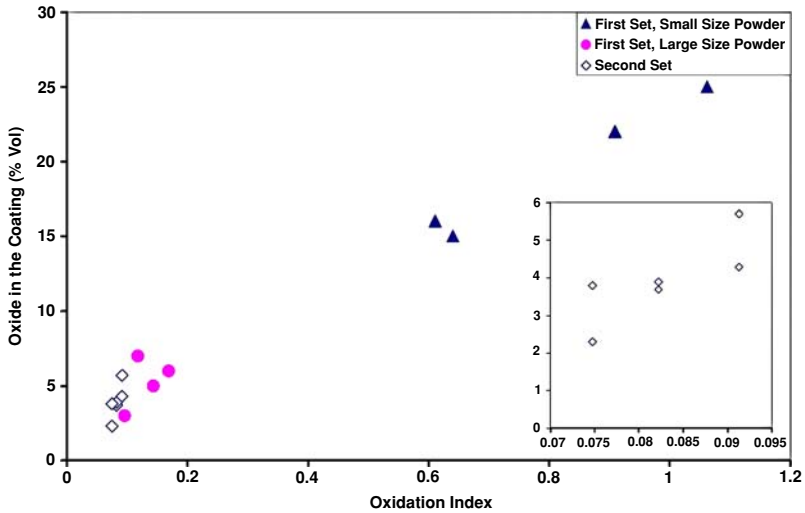

Fig. 14 The measured oxide volume fraction is plotted versus the calculated oxidation index for the APS coatings of alloy 625 for the first and second set of experiments. The inset shows the results for second set of experiments using an expanded scale

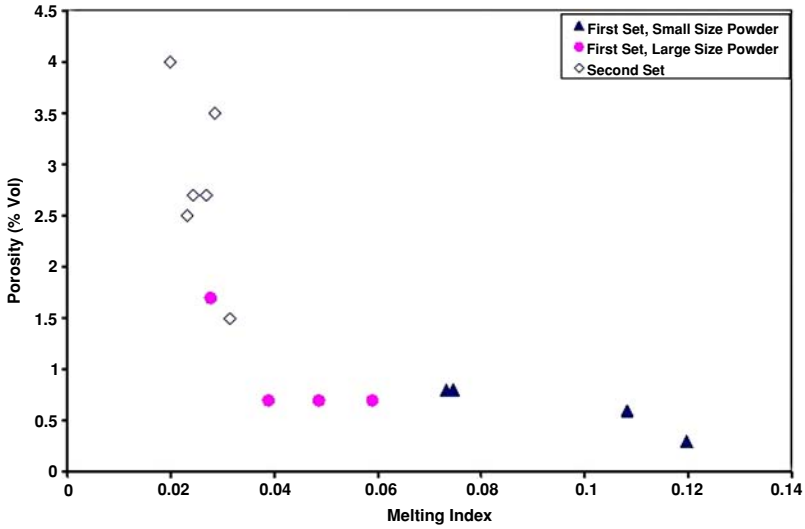

Fig. 15 The measured volume fraction porosity is plotted versus the calculated melting index for the APS coatings of alloy 625 for the first and second set of experiments

effects directly on porosity were spray distance, particle size, and current. Again, the effects of particle size and current can be attributed to their influence on the in-flight particle conditions, but the results showed no significant effect of spray distance on the in-flight characteristics. Two dimensionless parameters, the *oxidation index* and the *melting index*, incorporate all the parameters found to be significant in the statistical analyses. The *oxidation index* and the *melting index* correlated well with the measured oxide content and porosity, respectively, in the coatings.

References

1. F. Azarmi, Vacuum Plasma Spraying, *Adv. Mater. Process.*, 2005, **163**(8), p 37-40
2. P. Fauchais, Understanding Plasma Spraying, Institute of Physics Publishing, *J. Phys. D*, 2004, **37**, p 86-108
3. S. Sampath and H. Herman, Rapid Solidification and Microstructure Development During Plasma Spraying Deposition, *J. Therm. Spray Deposit.*, 1996, **5**(4), p 445-456
4. S. Guessasma, G. Montavon, and C. Coddet, Modeling of the APS Plasma Spray Process Using Artificial Neural Networks: Basis, Requirements and an Example, *Comput. Mater. Sci.*, 2004, **29**, p 315-333
5. J.A. Hearley, J.A. Little, and A.J. Sturgeon, The Effect of Spray Parameters on the Properties of High Velocity Oxy-fuel NiAl Intermetallic Coatings, *Surf. Coat. Technol.*, 2000, **123**, p 210-218
6. S. Sampath, X. Jiang, A. Kulkarni, J. Matejicek, D.L. Gilmore, and R.A. Neiser, Development of Process Maps for Plasma Spray: Case Study for Molybdenum, *Mater. Sci. Eng. A*, 2003, **348**, p 54-66
7. T.J. Steeper, W.L. Riggs II, A.J. Rotolico, J.E. Nerz, D.J. Varacalle Jr, and G.C. Wilson, A Taguchi Experimental Design Study of Plasma Sprayed Alumina-titania Coatings, *Proceedings of the Fourth National Spray Conference*, May 1991, Pittsburgh, PA, USA, p 4-10
8. J.R. Mawdsley, Y. Jennifer Su, K.T. Faber, and T.F. Bernecki, Optimization of Small-particle Plasma-sprayed Alumina Coatings Using Designed Experiments, *Mater. Sci. Eng. A*, 2001, **308**, p 189-199
9. S. Sampath, X.Y. Jiang, J. Matejicek, L. Prchlik, A. Kulkarni, and A. Vaidya, Role of Thermal Spray Processing Method on the Microstructure, Residual Stress and Properties of Coatings: An Integrated Study for Ni—5 wt.%Al Bond Coats, *Mater. Sci. Eng. A*, 2004, **364**, p 216-231
10. M. Friis, C. Persson, and J. Wigren, Influence of Particle In-flight Characteristics on the Microstructure of Atmospheric Plasma Sprayed Yttria Stabilized ZrO_2, *Surf. Coat. Technol.*, 2001, **141**, p 115-127
11. H. Singh, D. Puri, S. Prakash, and R. Maiti, Characterization of Oxide Scales to Valuate High Temperature Oxidation Behavior of Ni-20Cr Coated Superalloys, *Mater. Sci. Eng. A*, 2007, **464**, p 110-116
12. C. Zhou, J. Yu, S. Gong, and H. Xu, Influence of Water Vapor on the High Temperature Oxidation Behavior of Thermal Barrier Coatings, *Mater. Sci. Eng.*, 2003, **A348**, p 327-332
13. Y. Itoh, M. Saitoh, and Y. Ishiwata, Influence of High-temperature Protective Coatings on the Mechanical Properties of Nickel-based Superalloys, *J. Mater. Sci.*, 1999, **34**, p 3957-3966
14. R.K. Meyer and C.J. Nachtsheim, The Coordinate-exchange Algorithm for Constructing Exact Optimal Experimental Designs, *Technometrics*, 1995, **37**, p 60-69
15. A.A. Syed, A. Denoirjean, P. Denoirjean, J.C. Labbe, and P. Fauchais, In-flight Oxidation of Stainless Steel Particles in Plasma Spraying, *J. Therm. Spray Technol.*, 2005, **14**(1), p 117-124
16. H. Edris and D.G. McCartney, Microstructural Characterization of High Velocity Oxy-fuel Sprayed Coatings of Inconel 625, *J. Mater. Sci.*, 1997, **32**, p 863-872
17. H. Xiong, L. Zheng, L. Li, and A. Vaidya, Melting and Oxidation Behavior of In-flight Particles in Plasma Spray Process, *Int. J. Heat Mass Transfer*, 2005, **48**, p 5121-5133
18. A. Vaidya, G. Bancke, S. Sampath, and H. Herman, *Proceedings of the International Thermal Spray Conference (ITSC)*, C.C. Berndt, K. A. Khor Ed., ASM International, Materials Park, OH, 2001, p 1345-1349
19. E.A. Brandes and G.B. Brook, *Smithells Metals Reference Book*, 7th ed., Butterworth-Heinemann Ltd., 1992